Electronic Supplementary Material (ESI) for Physical Chemistry Chemical Physics.

Supplemental Material: Escape of Anions from Geminate Recombination in THF due to Charge Delocalization

Hung-Cheng Chen,[†] Andrew R. Cook,[†] Sadayuki Asaoka,[‡] Jeff Boschen,[⊥] Theresa Windus,[⊥] and John R. Miller[†,*]

[†]*Chemistry Department, Brookhaven National Laboratory, Upton, NY 11973, USA*

[‡]*Department of Biomolecular Engineering, Kyoto Institute of Technology, Matsugaskaki, Sakyo-ku, Kyoto 606-8585, Japan*

[⊥]*Department of Chemistry, Iwoa State University, Ames, Iwoa 50011, USA*

Section S1. Estimations of the Extinction Coefficients of the Anions

With an internal reference, the (Na^+,e_s^-) ion pair, ε=2.4×10^4 $M^{-1}cm^{-1}$ at 890 nm in THF,[4] the extinction coefficients (ε) of benzophenone radical anions ($BPhO^{\bullet-}$) and oligofluorene radical anions ($F_n^{\bullet-}$,n=1-4) were estimated. Here e_s^- is the solvated electron. 10 mM of sodium tetraphenylborate ($NaBPh_4$) was employed to provide ~938 μM of free Na^+ to form (Na^+,e_s^-) ion pair with a rate constant, 7.90×10^{11} $M^{-1}s^{-1}$.[4] With the dissociation equilibrium constant of $NaBPh_4$, 8.52×10^{-5} M, in THF at 298 K,[5] the concentration of free Na^+ is calculated. The lifetime of (Na^+,e_s^-) ion pairs is ~2 μs[4] so e_s^- could attach to BPhO and F_n(n=1-4) before recombination of e_s^- with solvated protons and THF radical cation. The free Na^+ also extends the lifetimes of $BPhO^{\bullet-}$ and $F_n^{\bullet-}$(n=1-4) so [$BPhO^{\bullet-}$] and [$F_n^{\bullet-}$(n=1-4)] are almost identical to the concentration of (Na^+,e_s^-) ion pairs after the electrons completely transfer from (Na^+,e_s^-) ion pairs to BPhO and F_n (n=1-4) during the observation time period.

In THF solutions, the ε of $BPhO^{\bullet-}$ was estimated by pulse radiolysis with 10 mM of $NaBPh_4$. In Figure S1.1a, kinetic traces of (Na^+,e_s^-) at 890 nm with and without 0.5 mM of BPhO show that electrons completely transfer from (Na^+,e_s^-) to BPhO after 1 μs. The kinetic trace of $BPhO^{\bullet-}$ at 700 nm with NaBPh4 shows that the lifetime of $BPhO^{\bullet-}$ is extended by Na^+. Therefore, ε of $BPhO^{\bullet-}$ at 700 nm is 9.0×10^3 $M^{-1}cm^{-1}$ estimated from ratio of absorbance between 2 ns and 2 μs with the assumption that numbers of (Na^+,e_s^-) and $BPhO^{\bullet-}$ are identical.

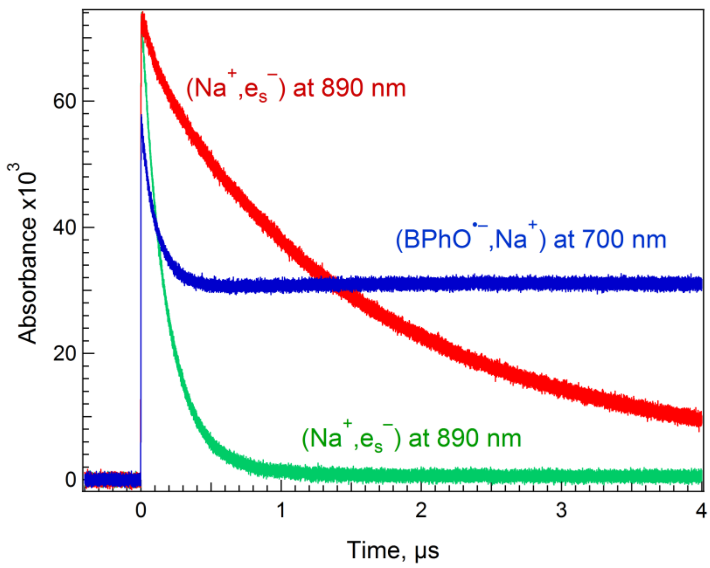

Figure S1.1 In THF solutions 10 mM of sodium tetraphenylborate ($NaBPh_4$) kinetic traces of (Na^+,e_s^-) ion pairs (Red) shows that the lifetime of (Na^+,e_s^-) ion pairs is ~2 μs. With addition of 0.5 mM of benzophenone (BPhO) (Na^+,e_s^-) decays faster to produce (Na^+,$BPhO^{•-}$).

The presence of Na^+ may shift the absorption bands of radical anions in THF. Transient spectra of $BPhO^{•-}$ with and without $NaBPh_4$ in THF shown in Figure S1.2 demonstrate that Na^+ shifts the absorption band of $BPhO^{•-}$ from 800 to 700 nm in THF. The oscillator strengths (*f*) of $BPhO^{•-}$ with and without $NaBPh_4$ from 600 to 1000 nm are 0.4176 and 0.4817. This suggests that these two absorption spectra are contributed by the same absorption band of $BPhO^{•-}$. Therefore, the ε of $BPhO^{•-}$ at 800 and ($BPhO^{•-}$,Na^+) at 700 nm are very similar.

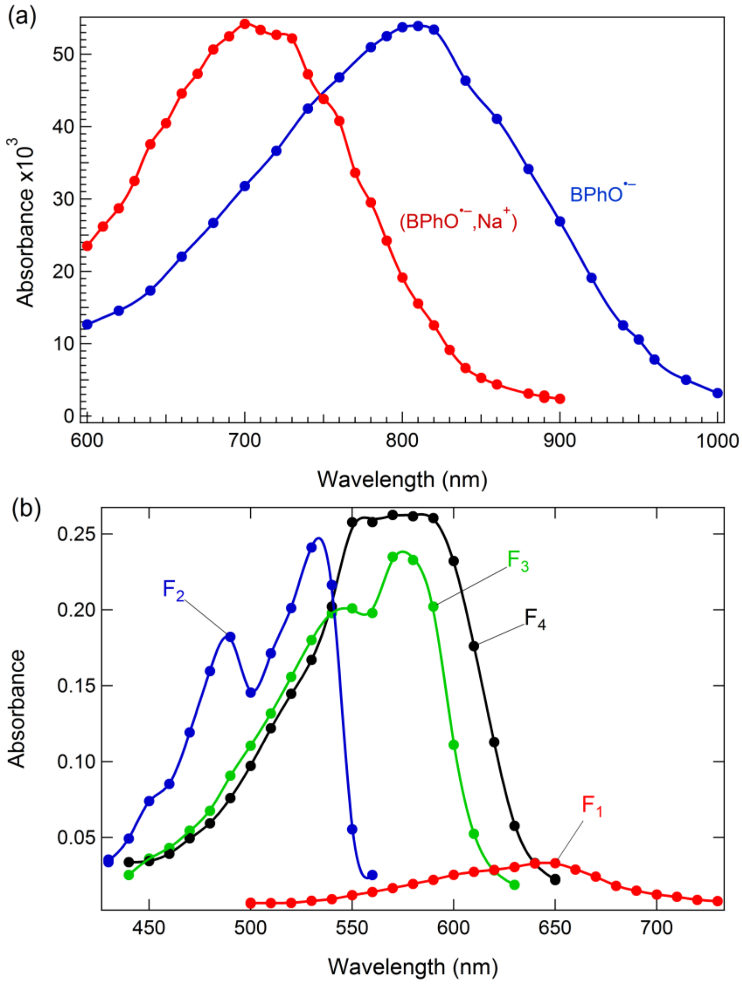

Figure S1.2 In THF, (a) transient spectra of benzophenone (BPhO, 0.5 mM) from pulse radiolysis with and without 10 mM of $NaBPh_4$; (b) transient spectra of F_n (n=1-4) from pulse radiolysis with 10 mM of $NaBPh_4$, and concentrations of F_n (n=1-4) are 0.4, 0.3, 0.2, and 0.2 mM.

With the method for estimating the ε of $BPhO^{•-}$, the ε of $F_n^{•-}$ (n=1-4) were estimated in 0.5, 0.4, 0.3, 0.2, and 0.2 mM of F_n(n=1-4) solutions; the results are given in Table 1. Comparing absorption spectra of $F_n^{•-}$ (n=1-4) given in Figure 3 to theose of $F_n^{•-}$ (n=1-4) in $NaBPh_4$ solutions shown in Figure S1.2b that show no obvious absorption band shift at observation wavelengths of $F_n^{•-}$ (n=1-4) in the presence of Na^+.

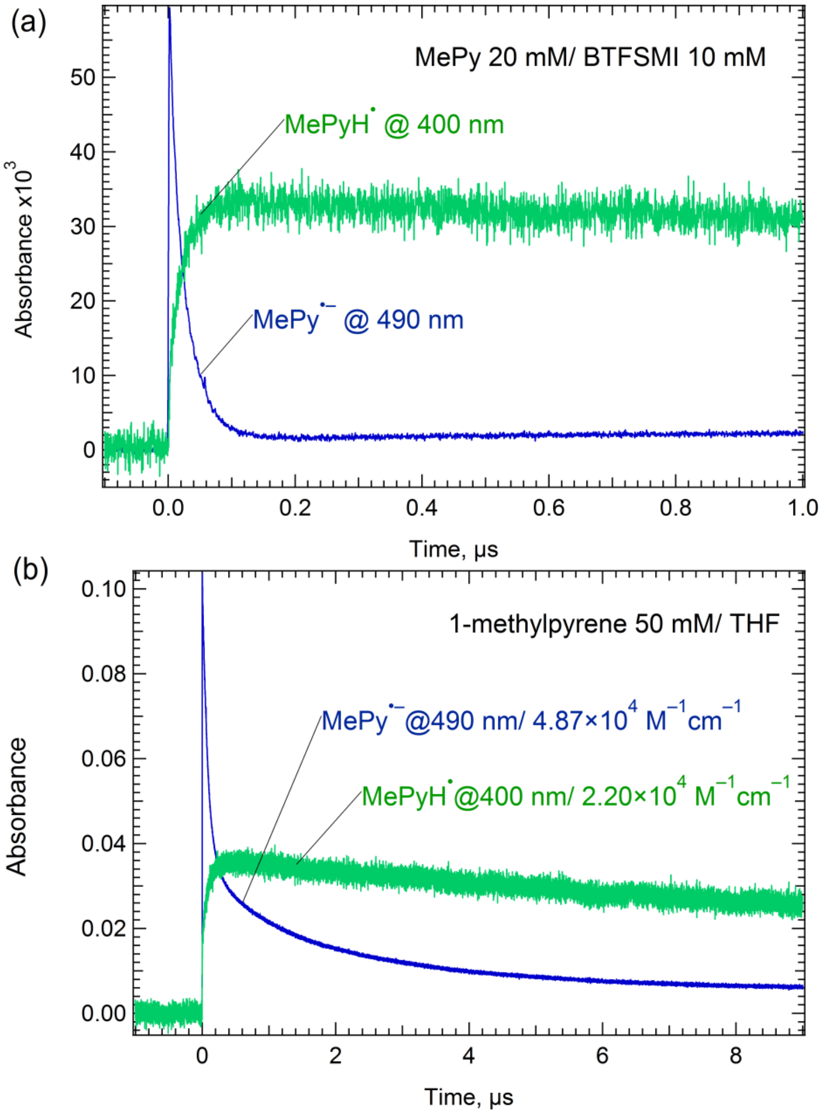

Figure S2. Kinetic traces after pulse radiolysis of 1-methylpyrene (MePy) at the 490 nm peak of $MePy^{\bullet-}$ and the 400 nm peak of $MePyH^{\bullet}$ (a) with 10 mM bis(trifluoromethane)sulfonimide (BTFSI) with MePy, and (b) MePy only in THF. The purpose of BTFSI is to quickly (<25 ns) protonate $MePy^{\bullet-}$ to form $MePyH^{\bullet}$. Because of this fast protonation nearly all $MePy^{\bullet-}$ were protonated to become $MePyH^{\bullet}$. With this assumption and the extinction coefficients of $MePy^{\bullet-}$ at 490 nm, $4.87(\pm0.29)\times10^{4}$ $M^{-1}cm^{-1}$ from Figure S5, we estimated the extinction coefficient of $MePyH^{\bullet}$ at 400 nm in THF to be $2.20(\pm0.13)\times10^{4}$ $M^{-1}cm^{-1}$. Based on these two extinction coefficients, the estimated yield of the geminate proton transfer (PT) reaction (Reaction 4b) seen in (b) is 0.86±0.12. This yield implies that in geminate recombination decay of the anions is likely due to the PT reaction with little contribution from electron transfer from $MePy^{\bullet-}$ to the solvated proton.

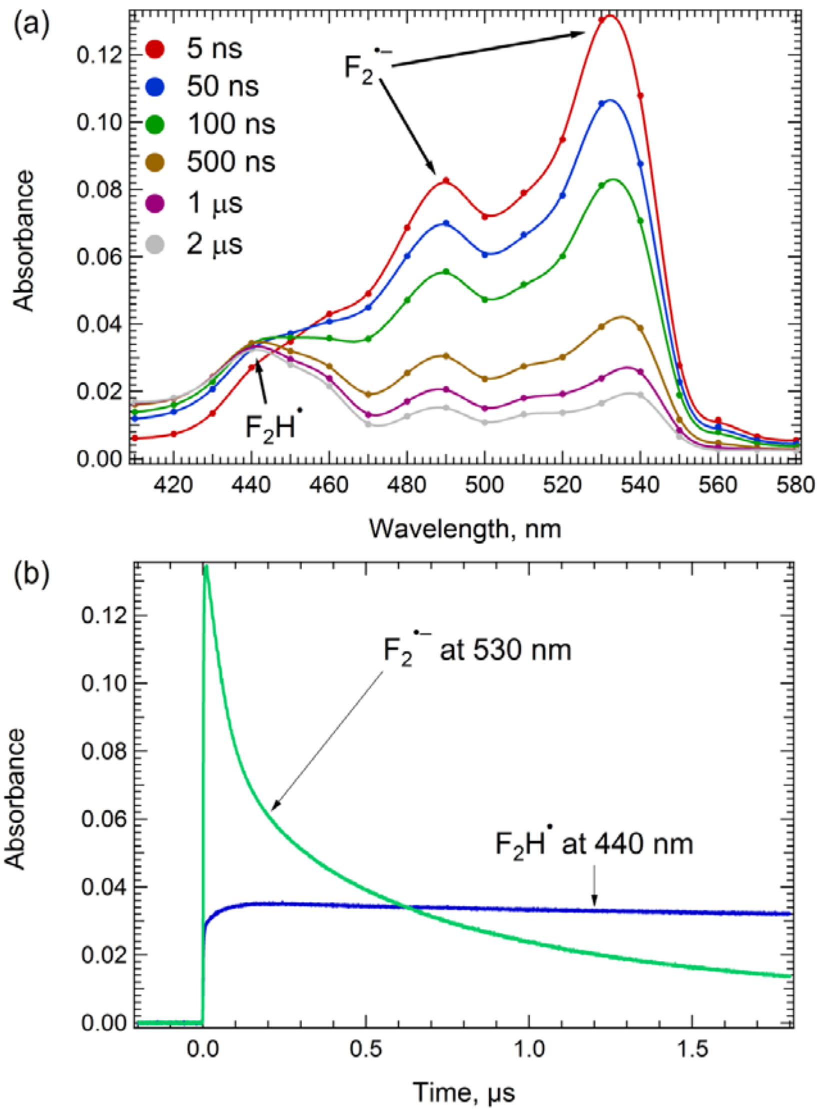

Figure S3. (a) Transient absorption spectra and (b) kinetic traces of $F_2H^{\bullet}$ and $F_2^{\bullet-}$ in THF solution with 8.4 mM of F_2 and 1 mM of HCl. The protonation of $F_2^{\bullet-}$ by HCl is slow, and $F_2H^{\bullet}$ mainly absorbs at 440 nm. At 440 nm the extinction coefficient of $F_2H^{\bullet}$ is barely larger than that of $F_2^{\bullet-}$, but growth can be observed during the most rapid part of the reaction.

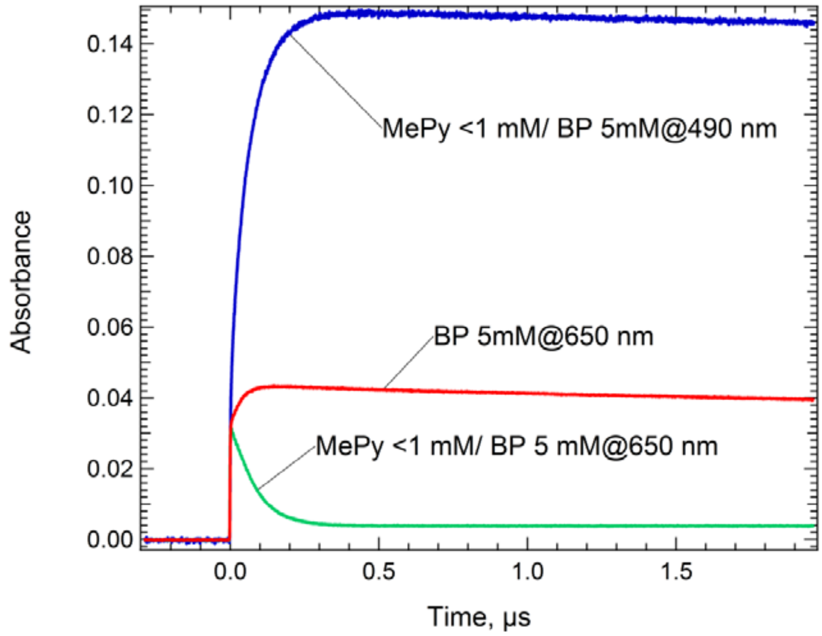

Figure S4 Kinetic traces of biphenyl (BP) with and without 1-methylpyrene (MePy) in 10 mM of tetrabutylammonium hexafluorophosphate ($TBAPF_6$) solutions. With the assumption that in the solution of BP + MePy, the conecntrations of $BP^{\bullet-}$ and $MePy^{\bullet-}$ are similar after 500 ns. Based on the extinction coefficient of $BP^{\bullet-}$, $1.26(\pm0.07)\times10^4$ $M^{-1}cm^{-1}$ at 650 nm,[6] the estimated extinction coefficient of $MePy^{\bullet-}$ is $4.87(\pm0.29)\times10^4$ $M^{-1}cm^{-1}$ at 490 nm. The kinetic trace of BP shows that $TBAPF_6$ enlogates the lifetime of $BP^{\bullet-}$ to >1 μs, and the kinetic trace of BP with MePy at 650 nm show that the electrons completely transfer from $BP^{\bullet-}$ to MePy within 400 ns.

Section S5. Estimation of the G Values

In radiation chemistry, the product yield is reported as the G value, which is expressed as the number of species form per joule of energy absorbed by the sample (mol/J). Based on the linear energy transfer model,[7] difference of the energies absorbed by different samples can be estimated based on the sample's density. From the G value of e_s^- in the standard solution comprising of 20 vol% of methanol, 80 vol% of water, and 0.1 M of NaOH, we estimated the G value of $BPhO^{\bullet-}$ in THF by

$$\mathrm{G}_{\mathrm{BPhO}} = \frac{\mathrm{G}_{\mathrm{std}}\, \varepsilon_{\mathrm{std}} \rho_{\mathrm{THF}} A_{\mathrm{BPhO}}}{\varepsilon_{\mathrm{BPhO}} \rho_{\mathrm{std}} A_{\mathrm{std}}} \quad \text{(S5.1).}$$

Here G_{BPhO} and G_{std} are the G values of $BPhO^{\bullet-}$ in THF and e_s^- in the standard solution; A_{BPhO} and A_{std} are absorbances of $BPhO^{\bullet-}$ in THF and e_s^- in the standard solution; ε_{BPhO} and ε_{std} are the extinction coefficients of $BPhO^{\bullet-}$ in THF and e_s^- in the standard solution; ρ_{THF} and ρ_{std} are the densities of THF and standard solution. Values of the extinction coefficients and densities are given in Table S5.1. With the G value of e_s^- in water reported by Bartels,[8] we extrapolate the G(t=0) value of e_s^- in the standard solution, which is 401.8(±28.1) nmol/J and then, by Equation S5.1, the G value of $BPhO^{\bullet-}$ in THF is calculated.

Table S5.1 List of the Extinction Coefficients and Densities (see text).

	ε_{std} ($M^{-1}cm^{-1}$)	ε_{BPhO} ($M^{-1}cm^{-1}$)[a]	ρ_{THF} (g/cm^3)	ρ_{std} (g/cm^3)
value	2.30×10^4	7.90×10^3	0.8892	1.0075

[a]From Section S1 of the Support Information.

Kinetic traces of 50, 100, and 200 mM of BPhO at 760 nm in THF were collected pulse radiolysis using the optical fiber single shot detection system, which is described elsewhere,[10] and by transient digitalizer methods are shown in Figure S6.1. These data indicate that the number of step captured electrons is increased with increasing concentration. Details of estimation are in section S6. Table S5.2 shows that by the electro attachment, highly concentrated BPhO capture electrons within 300 ps, and the difference of yield between 50 and 200 mM is 20%. Figure S6.1a shows that yields of $BPhO^{\bullet-}$ are almost identical after 1 ns, which suggest annihilation of $BPhO^{\bullet-}$ is diffusion-limited. These results also signal that the free ion yield in THF is not concentration-dependent.

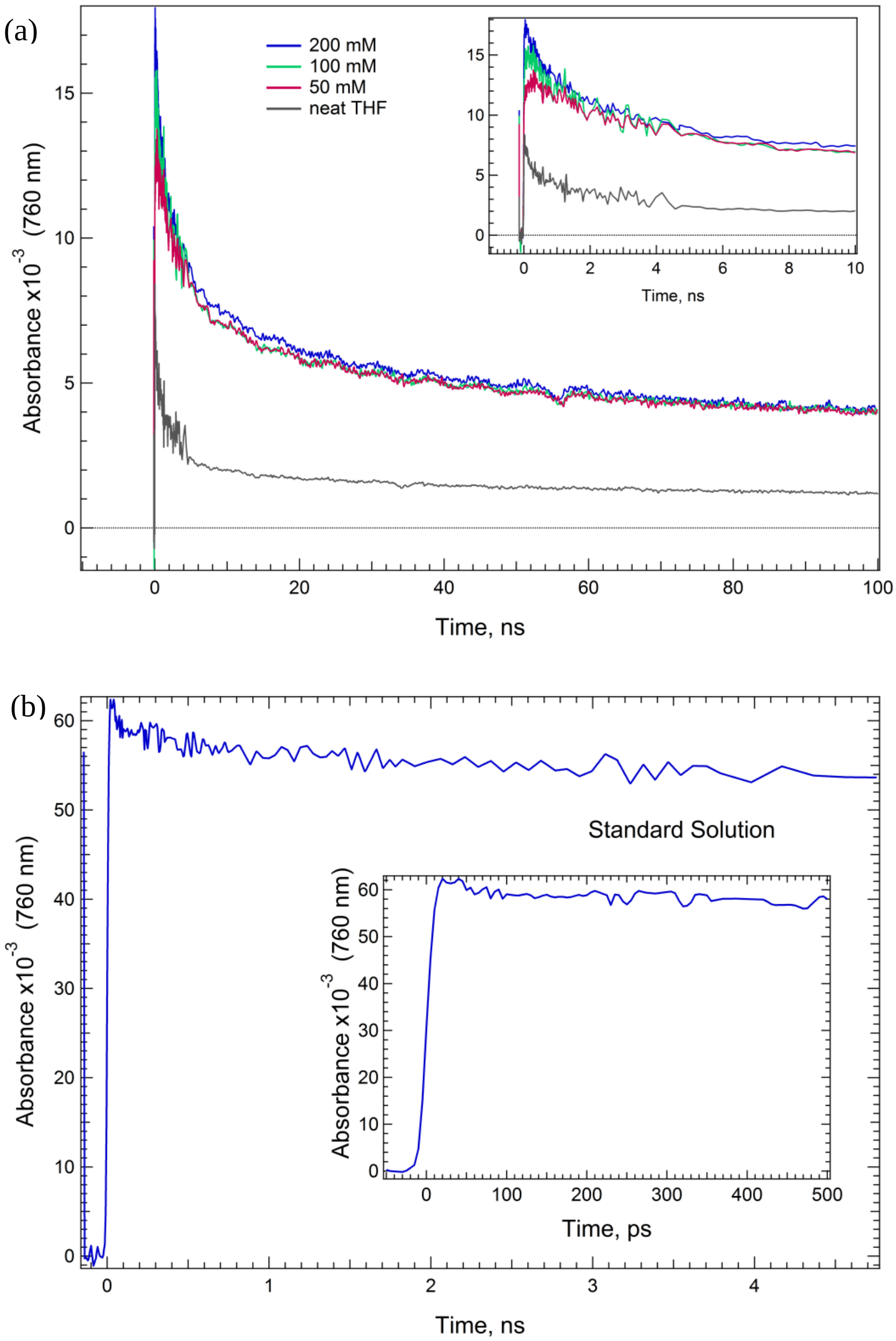

Figure S5.1 (a) Kinetic traces of $BPhO^{\bullet-}$ in 50, 100, and 200 mM of BPhO solutions and solvated electrons in THF at 760 nm were collected by optical fiber-based single shot[10] and transient digitalizer methods. (b) Kinetic trace of solvated electrons in standard solution at 760 nm collected by OFSS method.

From data shown in Figure S5.1a, averaged G_{fi} values of $BPhO^{\bullet-}$ in THF are 77.8(±4.9) nmol/J. By Equation S6.1 with parameters given in Table S5.1, and $A_{std}(t)$, $A_{BPhO}(t)$ given in Table S5.2, we calculated G(t) values of $BPhO^{\bullet-}$ in THF. Kinetic traces of different concentrations of BPhO were fitted by a four exponential function, $A_1\exp(-k_1t) + A_2\exp(-k_2t) + A_3\exp(-k_3t) + A_{fi}\exp(-k_4t)$, and then, with Equation S6.1, the fitting results were converted into the G values. Here A_i (i=1-3) and A_{fi} are the absorbances, and k_i (i=1-4) are the decay rates. The G_{fi} values of $BPhO^{\bullet-}$ are determined by Equation S6.1 with the A_{fi} absorbances.

Table S5.2 The Concentrations of Benzophenone (BPhO), the Absorbance of $BPhO^{\bullet-}$ at 800 nm, and the G(t) and G_{fi} values of $BPhO^{\bullet-}$.

Conc. (M)	$^{a}A_{std}(t)$	$^{b}A_{BPhO}(t)$	Time (ps)	$^{c,d}G_{max}$ (nmol/J)	$^{d}G_{fi}$ (nmol/J)
0.2	0.0592	0.017	60	328.1	86.2
0.1	0.0592	0.015	150	289.3	81.3
0.05	0.0592	0.013	280	251.2	71.6

[a]Obtained from Figure S6.1(b)
[b]Obtained from Figure S6.1(a)
[c]Calculated by equation S6.1
[d]9% of Uncertainty

Section S6. Estimation of the Captured Fractions of the Electrons

The electrons created by the pulse radiolysis method can be captured by the "step capture" process and electron attachment. The step captured fraction of the electrons (F_{sc}) can be estimated by:

$$F_{sc} = 1 - \exp(-q[s]) \qquad \text{(S6.1)},^{11\text{-}12}$$

where [s] is the concentration, and q is the quencher coefficient. The q values of BPhO and F_n (n=2-4) are given in Table S6.1. F_{sc} is the fraction of solvated electrons (e_s^-) are the surviving from the step capture and solvated by solvent molecules. In other words, the e_s^- fraction of the electrons is $1-F_{sc}$. Kinetic trace of e_s^- in THF shown in Figure S6.1 indicate that ~75% of e_s^- decay geminately with rate 9.70×10^8 s^{-1} (k_{gd}) and ~25% of e_s^- decay homogenously with rate 1.95×10^6 s^{-1} (k_{hd}). The capture e_s^- fraction of the electrons (F_s) are estimated by:

$$F_s = \left(0.75\cdot\frac{k_{att}[s]}{k_{att}[s]+k_{gd}} + 0.25\cdot\frac{k_{att}[s]}{k_{att}[s]+k_{hd}}\right)\cdot(1-F_{sc}) \qquad \text{(S6.2)},$$

where k_{att} is the attachment rate constant. The k_{att} of BPhO and F_n (n=2-4) are given in Table S7.1. The fractions of captured electrons of BPhO with different concentrations and F_n (n=2-4) are given in Table S6.1.

Table S6.1 Estimated fractions of the step-captured electrons (F_{sc}), captured solvated electrons (F_s) and total captured electrons (F_{tot}) by benzophenone with different concentrations and F_n (n=2-4)

Name	q (M^{-1})	k_{att} ($M^{-1}s^{-1}$)	Conc. (M)	$^{a}F_{sc}$	$^{b}F_s$	F_{tot}
Benzophenone	[c]11.5	[e]6.40×10^{10}	0.2	0.898	0.078	0.976
			0.1	0.683	0.285	0.968
			0.05	0.437	0.465	0.902
F_2	[d]13.8	[13]6.62×10^{10}	0.03	0.339	0.498	0.837
F_3	[d]20.7	[13]6.15×10^{10}	0.03	0.463	0.398	0.861
F_4	[d]27.6	[13]1.09×10^{11}	0.03	0.424	0.443	0.867

[a]Calculated by Equation S7.1 and see text.
[b]Calculated by Equation S7.2 and see text.
[c]Benzophenone and biphenyl are similar in the molecular size so we use the value of q from measurement on biphenyl[6] in THF for benzophenone.
[d]$q=nq_{rp}$. Here n is the length in the repeat units, q_{rp}=6.9 M^{-1} is the quenching coefficient per repeat-unit concentration from our previous work.[14]
[e]Obtained by observing decay of solvated electrons in THF solution directly.

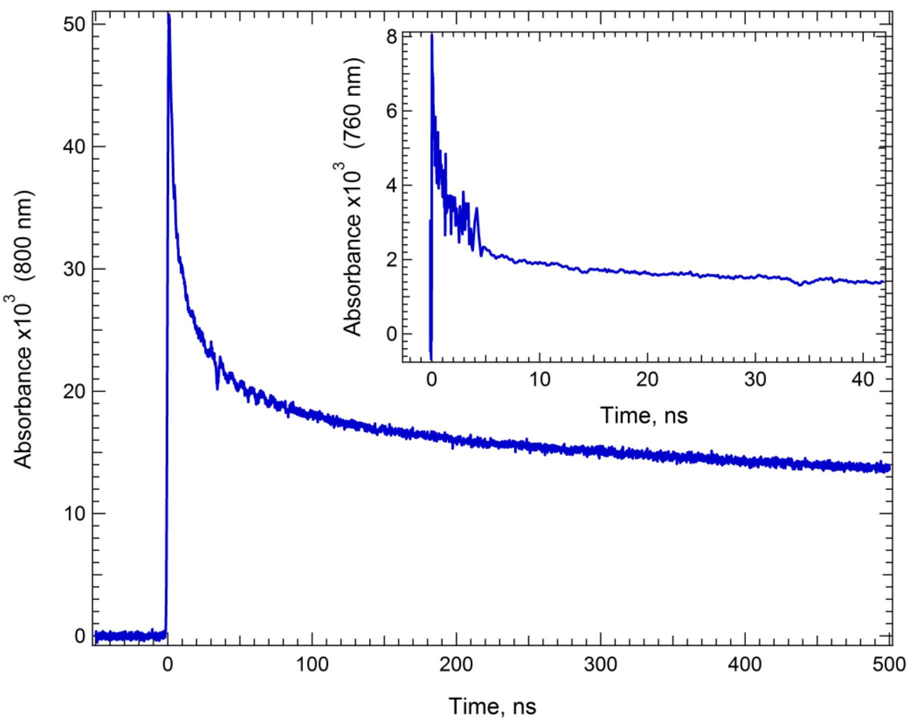

Figure S6.1 A kinetic trace of transient absorption of e_s^- in THF at 800 nm collected by the transient digitizer method with 2 ns time resolution from FND-100 photodiode. It indicates that homogenous decay rate of e_s^- is 1.95×10^6 s^{-1} in THF. The inset shows a kinetic trace of e_s^- at 760 nm collected by the optical fiber-based single shot[10] with 15 ps time resolution. It indicates that geminate decay rate of e_s^- is 9.70×10^8 s^{-1} in THF.

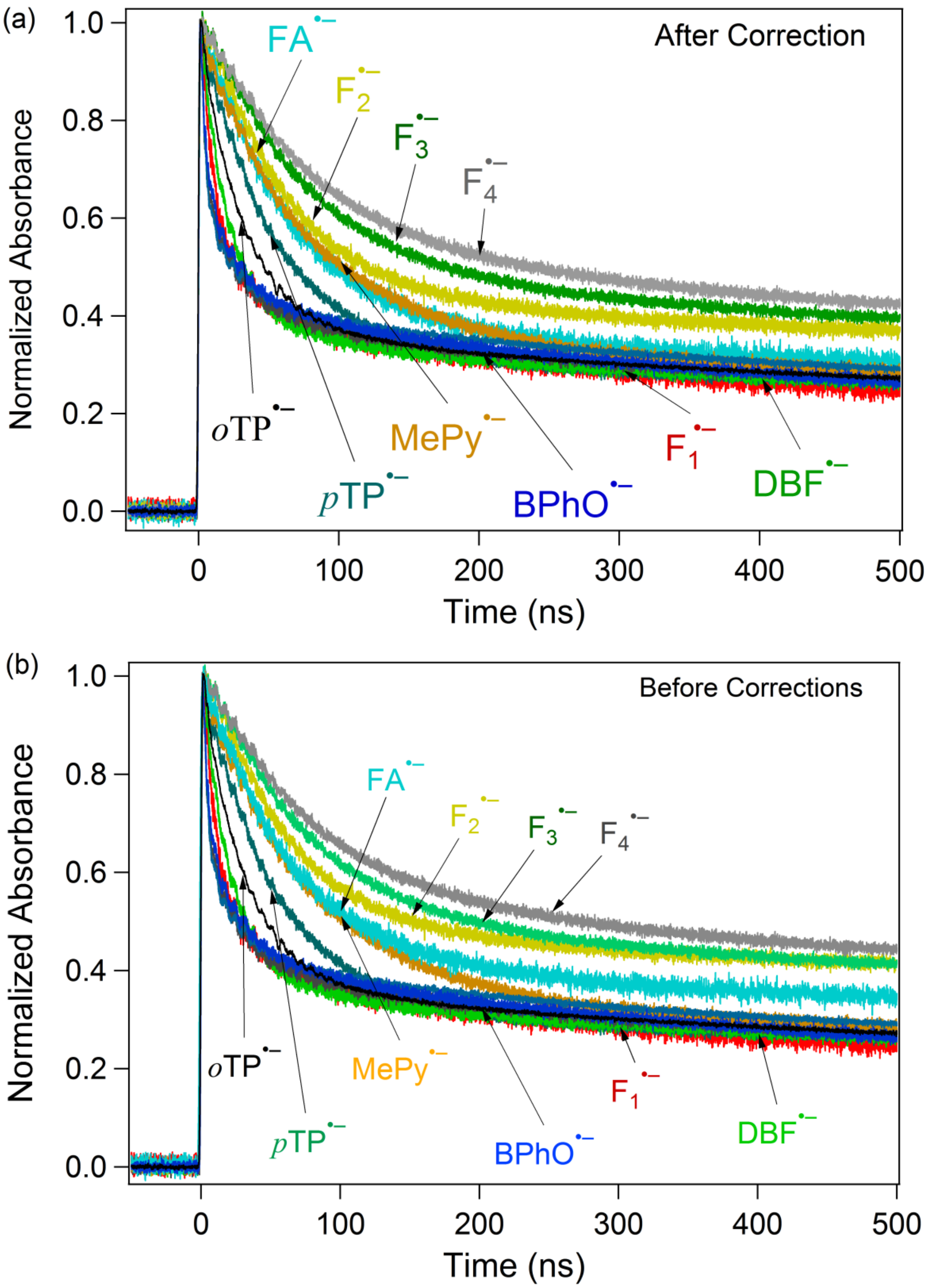

Figure S7 (a) Normalized kinetic traces of benzophenone (BPhO) at 800 nm, fluoranthene (FA) at 450 nm, 1-methylpyrene (MePy) at 490 nm, dibenzofuran (DBF) at 680 nm, *p*-terphenyl (*p*TP) at 950 nm, *o*-terphenyl (*o*TP) at 600 nm, F_1 at 650 nm, F_2 at 530 nm, F_3 at 570 nm, and F_4 at 580 nm. The normalization factors are 14.7, 30.1, 17.4, 27.0, 9.53, 15.6, 16.3, 8.4, 3.3, and 8.2. Kinetic traces of FA and F_n (n=2-4) are corrected for the triplet absorptions (see Figures S8-S11). (b) Normalized kinetic traces without corrections for triplet absorptions of FA and F_n (n=2-4).

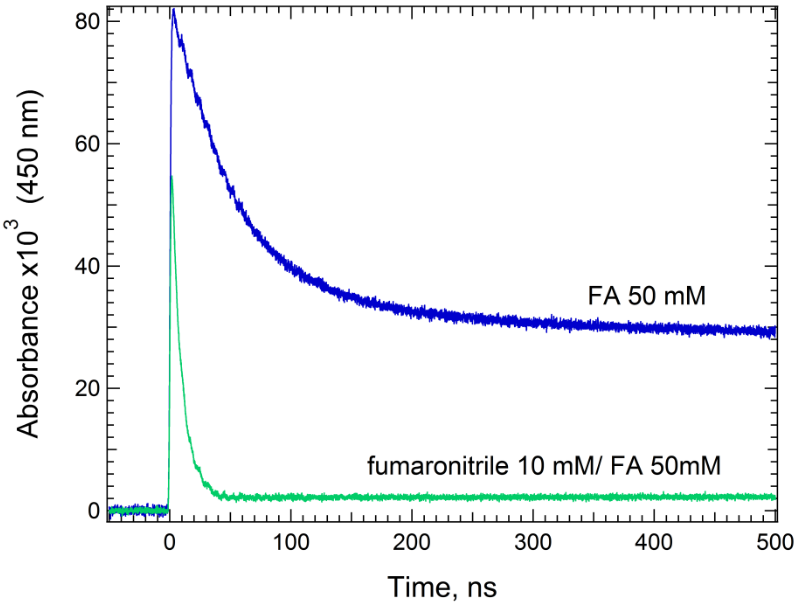

Figure S8 Kinetic traces of fluoranthene (FA) with and without 10 mM of fumaronitrile (FN) show that $^3FA^*$ absorbance is 5.5% of initial $FA^{\bullet-}$ absorbance at 450 nm in THF. The reduction potentials of FA[15] and FN[15] are −1.78 and −1.3 V (vs. SCE), so electrons will transfer from $FA^{\bullet-}$ to FN with a diffusion-limited electron transfer rate (k_{ET}), ~1.0×10^{10} s^{-1}. $^3FA^*$ has absorption at 450 nm with a decay rate (k_d), 2.0×10^6 s^{-1}.[16] Therefore, decay of the kinetic trace of FA with FN (green), which is faster than the k_t, is due to electron transfer from $FA^{\bullet-}$ to fumaronitrile. The initial absorbance (t=0) of $^3FA^*$ is extrapolated from data of FA with FN by a two-exponential function, $A_{\mathrm{ET}}\exp(-k_{\mathrm{ET}}t) + A_{\mathrm{t}}\exp(-k_{\mathrm{d}}t)$. Here A_{ET} and A_t are the absorbances. Based on this extrapolation and the initial absorbance, we estimate the ratio between absorbance of $FA^{\bullet-}$ and $^3FA^*$.

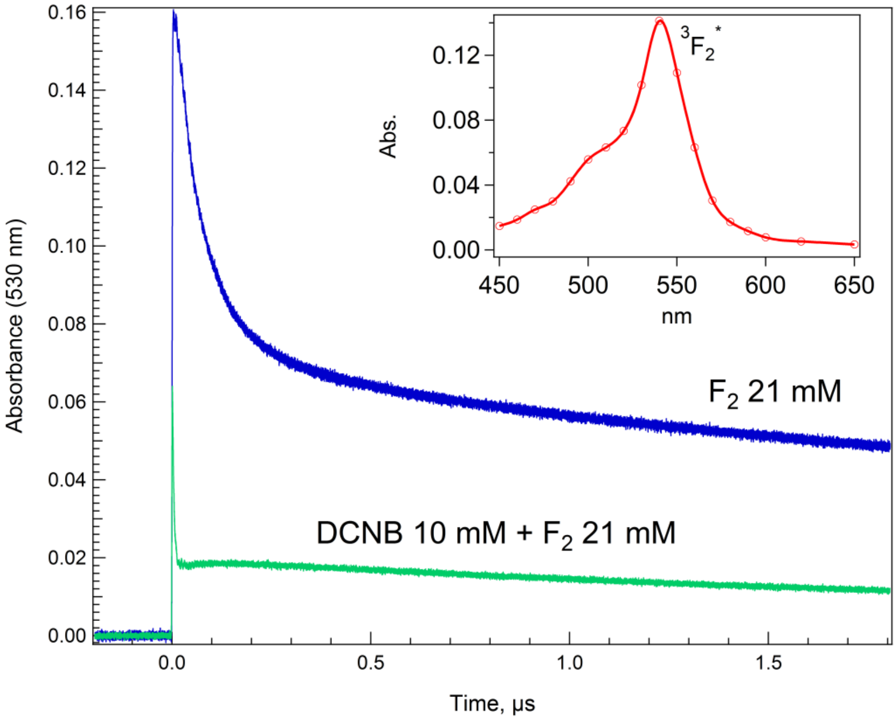

Figure S9 Kinetic traces of F_2 with and without *p*-dicyanobenzene (DCNB) show that $^3F_2^*$ absorbance is 7.1% of initial F_2 absorbance at 530 nm in THF. The inset is the absorption spectrum of $^3F_2^*$ in *p*-xylene. Based on that the reported reduction potential, $E^0(M^{0/-})$, of F_2 and DCNB are −2.33[17] and −1.52 V vs. SCE,[18] the electrons will transfer from $F_2^{\bullet-}$ to DCNB with a diffusion-limited electron transfer rate (k_{ET}), ~1.0×10^{10} s^{-1}. Therefore, the only species absorbing light is $^3F_2^*$ after electron transfer complete. The initial absorbance (t=0) of $^3F_2^*$ is extrapolated from data of F_2 with DCNB by a two-exponential function. Based on this extrapolation and the initial absorbance of F_2, we estimate the absorbance ratio between $F_2^{\bullet-}$ and $^3F_2^*$.

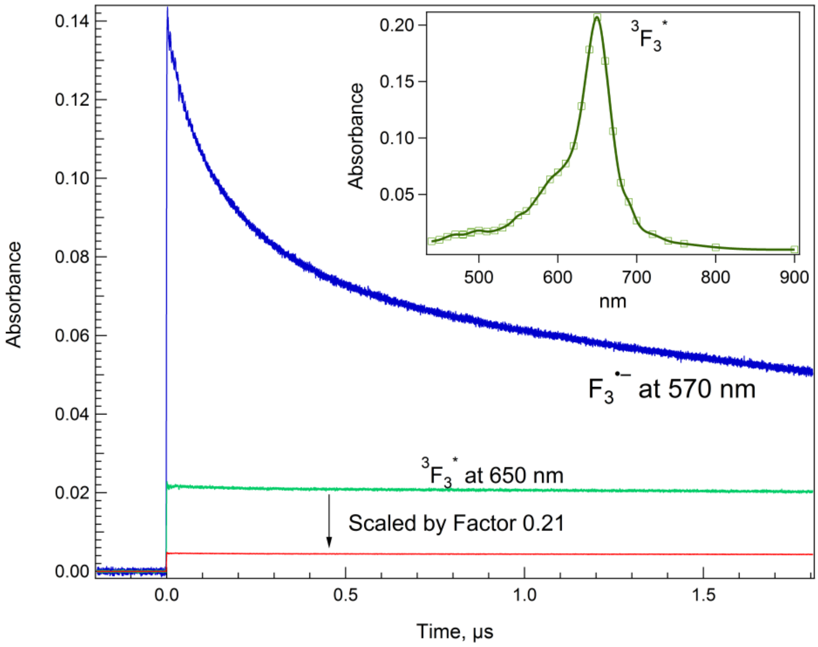

Figure S10 Kinetic traces 20 mM F_3 in THF solution at the 570 nm maximum of $F_3^{\bullet-}$ and at the 650 nm maximum of $^3F_3^*$. $^3F_3^*$ shows no decay on this time scale. The inset is the absorption spectrum of $^3F_3^*$ in *p*-xylene, from which A_{570}/A_{650} is 0.21, where A_λ is the absorbance at wavelength λ. Based on this absorbance ratio, ~3.3% of the initial absorbance at 570 nm is contributed by $^3F_3^*$.

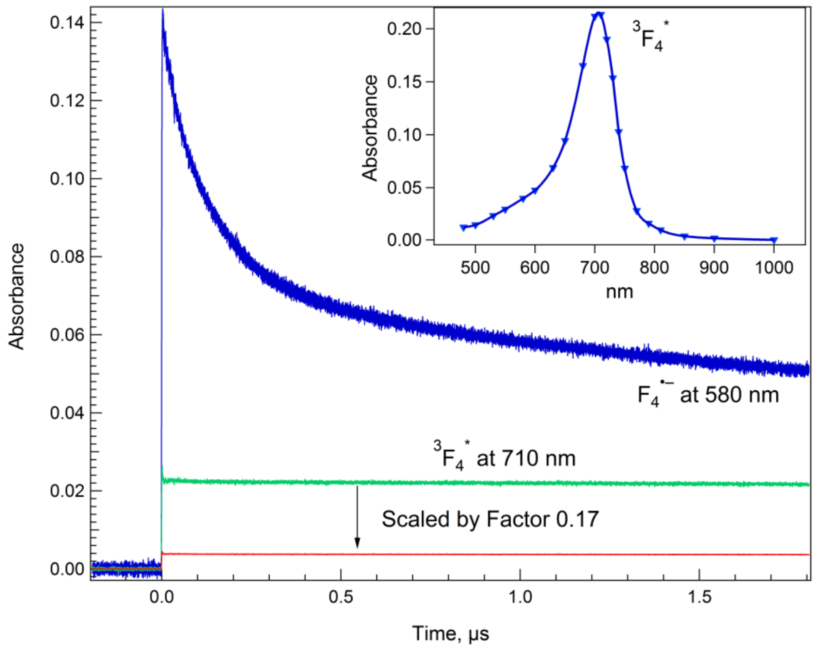

Figure S11 Kinetic Trances of $F_4^{\bullet-}$ and $^3F_4^*$ are collected at 580 nm and 710 nm in THF soulution with $[F_4]$=20 mM. The inset is absorption spectrum of $^3F_4^*$ in *p*-xylene, which shows that A_{580}/A_{710} is 0.17, where A_λ is the absorbance at wavelength λ nm. Based on this absorbance ratio, we estimate that ~3% of initial absorbance at 580 nm is contributed by $^3F_4^*$.

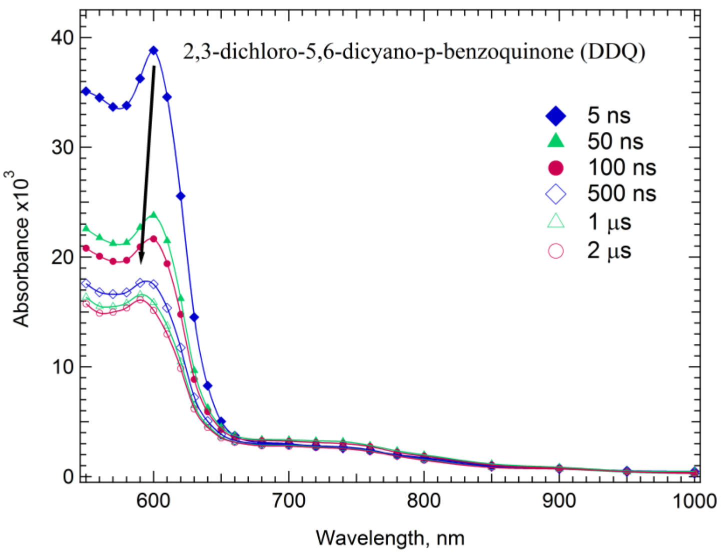

Figure S12 Transient spectra of 2,3-dichloro-5,6-dicyano-p-benzoquinone radical anion ($DDQ^{\bullet-}$) in THF with [DDQ]=50 mM. At 5 ns $DDQ^{\bullet-}$ has a peak at 600 nm that appears to shift to ~590 nm at 1 μs. This may be due to an impurity reacts with free $DDQ^{\bullet-}$ that may interfere our obervations to the free ion yield.

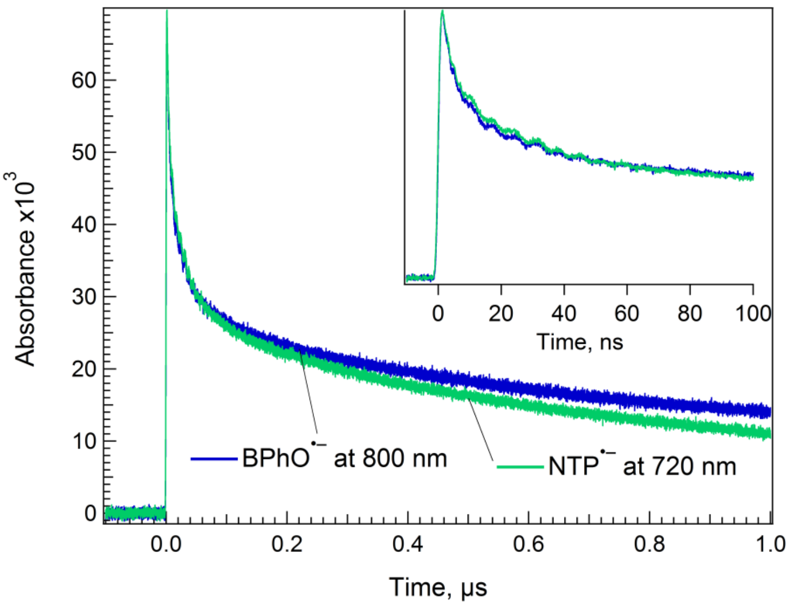

Figure S13 Normalized kinetic traces of benzophenone anion ($BPhO^{\bullet-}$) and 4-nitro-*p*-terphenyl anion ($NTP^{\bullet-}$) in THF show that geminate decay of $NTP^{\bullet-}$ is ~8 ns which is as fast as that of $BPhO^{\bullet-}$. The concentrations of BPhO and NTP are 50 mM. The kinetic traces of $BPhO^{\bullet-}$ and $NTP^{\bullet-}$ are multiplied by 14.7 and 24.6, respectively. From Table S15.1, $E^0(BPhO^{0/-})= -1.926$ V vs. SCE, and $E^0(NTP^{0/-})=-1.14$ V vs. SCE.

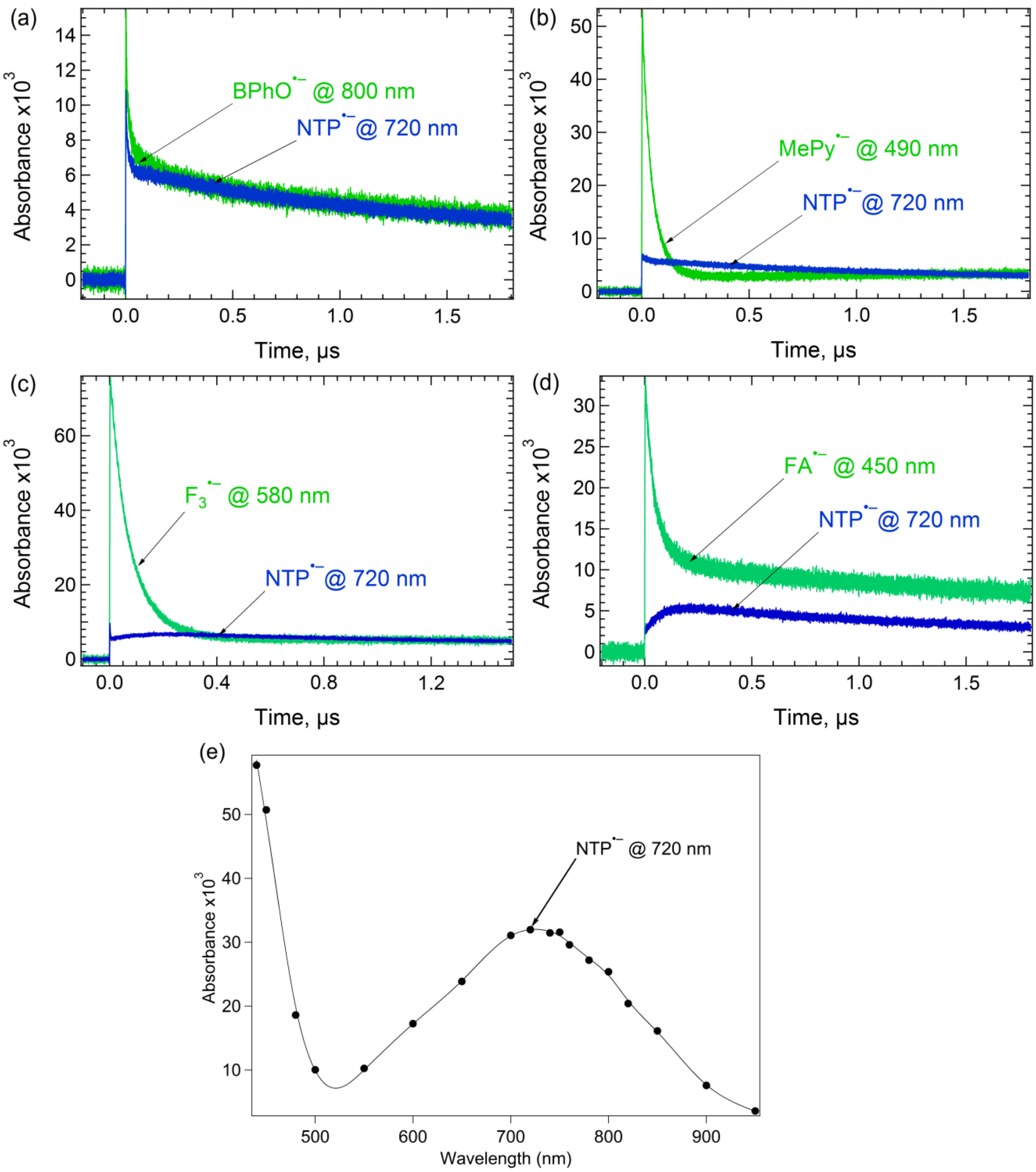

Figure S14 Kinetic traces of (a) benzophenone (BPhO, 50 mM), (b) 1-methylpyrene (MePy, 50 mM), (c) F_3 (20 mM), (d) fluoranthene (FA, 50 mM), with 4-nitro-p-terphenyl (NTP, 1 mM) in THF, and (e) Absorption spectrum of the NTP radical anion in THF. These kinetics show that the BPhO, MePy, and FA radical anions transfer to NTP within 200 ns. For F_3 anions the decay takes almost twice as long.

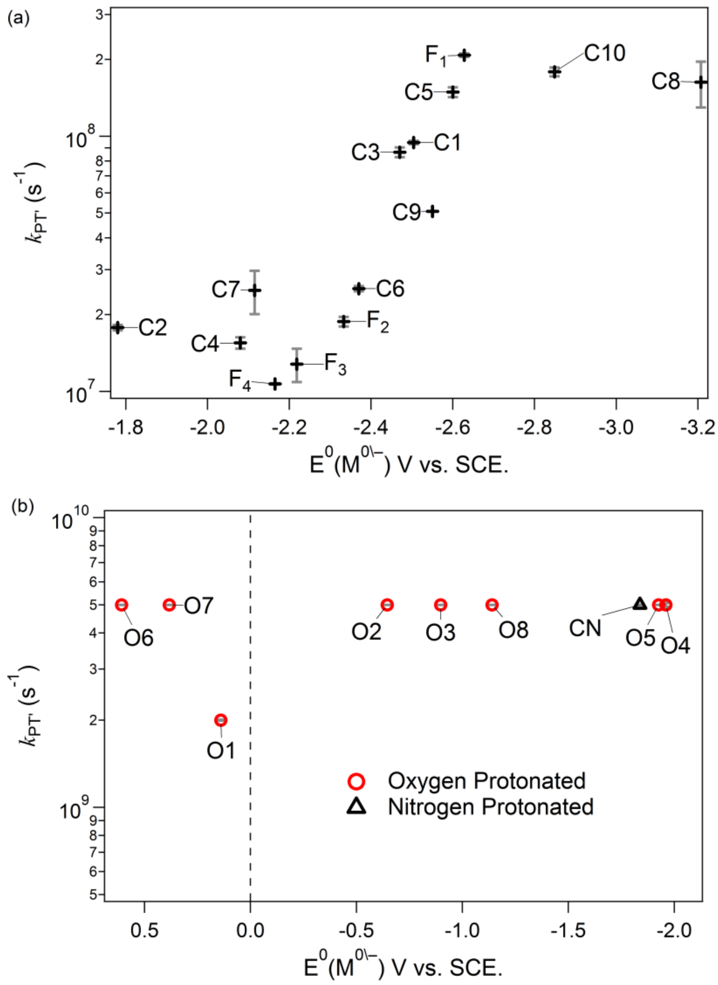

Figure S15 Plots of the measured proton transfer rate constant ($k_{PT'}$) vs. the reduction potential ($E^0(M^{0/-})$) for (a) the C protonated and (b) O and N protonated molecules. The values of the $E^0(M^{0/-})$ vs. SCE are in Table S16.1.

Section S16. Calculations of the Standard Free Energy Change (ΔG^0)

Proton Transfer Reaction. The proton transfer (PT) reaction (Reaction 4a) are separated into four half-reactions:

$M^{\bullet-}{}_{(liq)} \rightarrow M_{(liq)} + e^{-}{}_{(gas)}$	(Electron Detachment)	(5)
$RH_2^{+}{}_{(liq)} \rightarrow RH_{(liq)} + H^{+}{}_{(gas)}$	(Solvated Proton Dissociation)	(6)
$e^{-}{}_{(gas)} + H^{+}{}_{(gas)} \rightarrow H^{\bullet}{}_{(gas)}$	(Charge Recombination)	(7)
$M_{(liq)} + H^{\bullet}{}_{(gas)} \rightarrow MH^{\bullet}{}_{(liq)}$	(H Atom Addition)	(8).

Here M is the solute molecue, RH_2^+ is the solvated proton, RH is THF, and $MH^{\bullet}$ is the product of the PT reaction. The ΔG^0 of the PT reaction is sum of the ΔG^0 of Reactions 5-8 (ΔG_i^0, i=5-8). The ΔG^0 of Reactions 5 and 7 are calculated based on experimental results, and those of Reactions 6 and 8 are calculated by computation.

We calculated the ΔG_5^0 by using the reduction potential ($E^0(M^{0/-})$ vs. SCE) of the solute molecule measured by the electrochemistry substrating the Fermi level of the reference electrode. Reported $E^0(M^{0/-})$ are given in Table S16.1, and the Fermi level of SCE is −4.71 eV.[19] The ΔG_7^0 in gas phase is −13.61 eV reported by Wagman and coworkers.[20]

Table S16.1 Reduction potentials $E^0(M^{0/-})$ V vs. SCE, free energies for hydrogen atom Addition (ΔG_8^0), computed standard free cnergy change (ΔG^0) based on the reduction potential for the proton transfer reaction, and type of protonated atom (PA)

Symbol	Name (PA)[b]	$E^0(M^{0/-})^{Ref}$ (V)	ΔG_8^0 (eV)	ΔG^0 (eV)
F_1	F_1 (C)	−2.628[17]	−0.686	−1.581
F_2	F_2 (C)	−2.333[17]	−0.705	−1.245
F_3	F_3 (C)	−2.218[17]	−0.705	−1.069
F_4	F_4 (C)	−2.165[17]	−0.705	−1.027
C1	dibenzofuran (C)	−2.504[21,f,q]	−0.769	−1.540
C2	fluoranthene (C)	−1.78[22,i,q]	−1.141	−1.188
C3	phenanthrene (C)	−2.47[22,o,q]	−0.831	−1.568
C4	1-methylpyrene (C)	−2.08[22,o,q]	−0.998	−1.345
C5	biphenyl (C)	−2.60[22,o,q]	−0.574	−1.442
C6	*p*-terphenyl (C)	−2.37[23,j,q]	−0.584	−1.221
C7	terthiophene (C)	−2.115[24,k]	−0.528	−0.910
C8	fluorobenzene (C)	−3.207[25,l]	−0.506	−1.980
C9	*o*-terphenyl (C)	−2.55[23,j,q]	−0.570	−1.318
CN	4-cyano-4’-*n*-pentyl-*p*-terphenyl (N)[e]	−1.838±0.014[c]	−0.656[d] −0.101[e]	−0.761[d] −0.206[e]
O1	*p*-dinitrobenzene (O)	−0.645[26,m,q]	−1.361	−0.273
O2	benzophenone (O)	−1.926[21,f,q]	−1.004	−1.197
O3	anthraquinone (O)	−0.816[27,n,q]	−1.380	−0.453
O4	tetrachloro-*p*-benzoquinone (O)	0.14[27,n,q]	−2.184	−0.311
O5	acetophenone (O)	−1.96[28,o,q]	−0.779	−1.006
O6	[a]DDQ(O)	0.608[27,n,q]	−2.412	−0.061
O7	4-nitro-*p*-terphenyl (O)	−1.14[29,p,q]	−1.313	−0.720
O8	2,3-dicynao-*p*-benzoquinone (O)	0.383[27,n,q]	−2.454	−0.338
N	tetracynaoethene (N)	0.18[30,p,q]	−1.104	0.809

[a] 2,3-dicynao-5,6-dichloro-*p*-benzoquinone

[b] The protonated atom (PA) is the atom for which the $MH^•$ created by proton transfer has the lowest energy based on single point energy computations.

[c] Based on $E^0(CNTP^{0/-})-E^0(AO^{0/-})$=0.122±14 mV measured by the bimolecular electron transfer equilibria method and $E^0(AO^{0/-})$=−1.96 V vs. SCE given in Table 3, we estimated the $E^0(CNTP^{0/-})$. Here CNTP and AO are the abbreviations of 4-cyano-4’-*n*-pentyl-*p*-terphenyl and acetophenone.

[d] Proton transfer to the 3 position of the *p*-terphenyl group gives the lowest single point energy.

[e] Proton transfer to N of the C≡N may give more favorable of kinetics.

[f] $E^0(M^{0/-})$ vs. Ag/AgCl (−0.045 V vs. SCE)[31] in dimethylformamide (DMF).

footnotes continnuted on the next page.

[i] $E^0(M^{0/-})$ vs. Hg pool (−0.55 V vs. SCE)[22] in DMF with tetra-*n*-butylammonium iodide (TBAI).

[j] $E^0(M^{0/-})$ vs. Ag/$AgNO_3$ in DMF converted to vs. SCE with the differences between biphenyl (BP) and *p*-/*o*-terphenyls from Ref. [23] and $E^0(BP^{0/-})$=−2.05 V vs. Hg pool.[22]
[k] $E^0(T_3^{0/-})$ vs. Ag/AgCl (−0.045 V vs. SCE)[31] was measured in dimethylamine (DMA) with tetra-*n*-butylammonium bromide (TBABr). Here T_3 is the abbreviation of terthiophene. Because the dielectric constants of DMA and THF are close, $E^0(T_3^{0/-})$ in these two solvents are assuming to be close.
[l] With $E^0(FBz^{0/-})-E^0(Bz^{0/-})$=0.173 V in THF from Ref. [25] and $E^0(Bz^{0/-})$=−3.38 V vs. SCE,[32] the $E^0(FBz^{0/-})$ is calculated. Here FBz and Bz are the abbreviations of fluorobenzene and benzene.
[m] Reported $E^0(M^{0/-})$ vs. ($CoCp_2^{0/+}$) in THF with $TBAPF_6$ and converted into *vs*. SCE from $E^0(Fc^{0/+})$=1.332 V,[26] $E^0(DNB^{0/-})$=−0.124 V,[26] $E^0(AQ^{0/-})$=−0.125 V,[26] which three are *vs*. $CoCp_2^{+/0}$, and $E^0(Fc^{0/+})$=0.56 V[33] vs. SCE. Here $CoCp_2$, $TBAPF_6$, Fc, DNB, and AQ are the abbreviations of ccobaltocene, tetra-*n*-butylammonium hexafluorophosphate, ferrocene, *p*-dinitrobenzene, and anthraquinone.
[n] Reported $E^0(M^{0/-})$ vs. SCE in DMF with tetra-*n*-butylammonium tetrafluoroborate.
[o] Reported $E^0(M^{0/-})$ vs. SCE in DMF with TBAI.
[p] Reported $E^0(M^{0/-})$ vs. SCE in DMF with tetra-*n*-butylammonium perchlorate.
[q] $E^0(M^{0/-})$ in THF may be ~0.11-0.15 V more negative than $E^0(M^{0/-})$ in DMF.[26, 33]

Method Selection. Restricted-open MP2 (ROMP2) was selected to calculate the ΔG^0 of Reactions 6 and 8. For benzene, an experimental value of ΔG^0 of Reaction 8 in gas phase from falsh photolysis is −0.67 eV.[34] We are not aware of reports of the ΔG^0 of reaction 8 for other molecules. Therefore, we used benzene as a reference to selecte the computation method. Computation results from ROMP2, HF, B3LYP, and long-range corrected ωB97x (ω=0.3 Bohr^{-1}) with 6-31G(d) basis set, and G3 are in Table S15.2. From this table, ROMP2 gave the best agreement with the experiment is different by 0.17 eV. To overcome difficulty in optimizing geometry by ROMP2 (In Gaussian 09 D.1, ROMP2 is only capable of optimizing a molecule with less than 60 internal coordinates), a compromise is that the geometry optimized by B3LYP then the single point energy computed by ROMP2.

Table S16.2 Experimental and Calculated ΔG of Reaction 8 for Benzene in Gas Phase.

method	Exp.	^{a,b}ROMP2	^{a}B3LYP	^{a}HF	G3	^{a,c}ωB97x
benzene	-0.67 eV[34]	-0.499 eV	-1.222 eV	-1.318 eV	-1.009 eV	-1.256 eV

^{a}Basis set is 6-31G(d).
^{b}Restricted-open MP2 (ROMP2) with geometry optimized by B3LYP.
^{c}Long-range corrected ωB97x with ω=0.3 Bohr^{-1}

Solvated Proton Dissociation. The ΔG^0 of Reaction 6 was calculated by ROMP2 with the following procedures. Geometry of the solvated proton was optimized by B3LYP with the PCM solvation model in THF and corrections for the basis set superposition error (BSSE). Because the solvated proton is a weakly bound molecular complex, its computed geometry may be affected by BSSE leading to an artificial shortening of intermolecular distance. With this optimized geometry, the single point energy (SPE) was calculated by MP2, and the solvation energy is difference of the SPE calculated by B3LYP with and without the PCM solvation model in THF.

The solvated proton complex may contain one[7], two or more THF molecules. For most PT reactions, the complex where one proton stabilized by two THF molecules makes most PT reactions endoergic in disagreement with our observations that show occurrence of the PT reactions. While this disagreement may be related to errors in the calculated quantities, we utilize calculated ΔG_6^0 =10.643 eV for the complex in which one THF molecule stabilizes the proton. Possible structures of solvated proton complexes where the proton is stabilized by one and two THF molecules are shown in Figure S15.1.

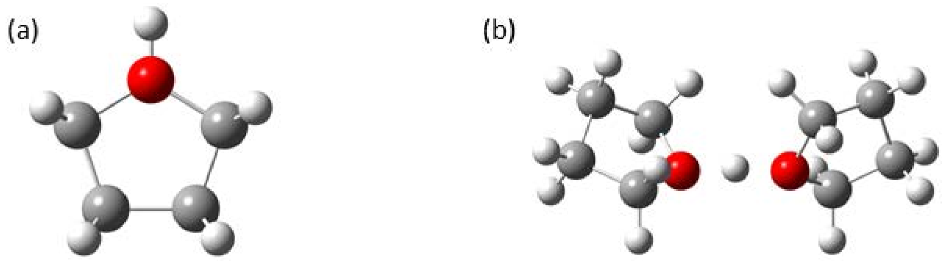

Figure S16.1 The solvated proton where the proton stabilized by (a) one and (b) two THF molecules.

Hydrogen Atom Addition. ΔG_8^0 was calculated by the following processes. Geometries and solvation energies of neutral and protonated molecules were optimized by B3LYP with the PCM solvation model in THF. Single point energies were then computed by restricted open MP2 in gas phase. The calculation results for the molecules studied here are given in Table S15.3. Details of estimating uncertainty for the calculated ΔG_8^0 are the following paragraphs.

In water, the proton transfer reaction (reaction 4a) will be

$$M^{\bullet -} + H_3O^+ \rightarrow MH^{\bullet} + H_2O \quad \text{(S16.1)}$$

which is in the opposite reaction direction of the acid dissociation reaction of $MH^{\bullet}$ in water. Here $MH^{\bullet}$ is a neutral radical and $M^{\bullet -}$ is radical anion. Therefore, the standard free energy change (ΔG^0) of Reaction S16.1 can be estimated based on the pK_a in water. Again, we sepearated reaction S16.1 into four half-reactions as reactions 5-8, but the reaction 6 is replaced by

$$H_3O^+_{(liq)} \rightarrow H_2O_{(liq)} + H^+_{(gas)} \quad \text{(S16.2)}$$

ΔG^0 of reaction S16.1 is estimated by the reduction potentials $E^0(M^{0/-})$ minus the Fermi energy on the reference electrode in liquid state, −4.71 eV [19] for SCE. The proton affinity of water is 7.229 eV reported by Collyer and McMahon,[35] and the solvation energies of H_3O^+ and H_2O in water are −4.490 and −0.274 eV.[36] Based on these values, ΔG^0 of reaction S15.2 is 11.445 eV.

Based on the reported pKa and $E^0(M^{0/-})$, ΔG^0 of reaction 8 (ΔG_8^0) can be estimated by:

$$\Delta G_8^0 = k_B T \ln(10^{-pK_a}) - [E^0(M^{0/-}) + 4.71] - 11.445 + 13.61\ eV \quad \text{(S16.3)},$$

where k_B is the Boltzmann constant, and T is temperature. Based on the pKa's and $E^0(M^{0/-})$ given in Table S15.3, by Equation S4.3, the ΔG_8^0 of AQ, AO, and BPhO in water can be calculated. The ΔG_8^0 of AQ, AO, and BPhO in water based on the experimental results and computations are in Table 16.3; Figure 16.1 shows a plot of the relative position of the ΔG_8^0 in water for these molecules. This plot shows that the experimental and calculated ΔG_8^0 differences from one molecule to another molecule are within 200 meV, but the computed values are more positive than the experimental values by an average of +0.9 eV.

Table 16.3 The pKa's, reduction potential $E^0(M^{0/-})$, Experimental, and Computed ΔG_8^0 in Water.

Name	pK_a^{Ref}	$E^0(M^{0/-})^{Ref}$ vs. SCE	experimental	calculated
benzophenone	9.25[37]	−1.184 V[37,38]	−1.906 eV	−1.002 eV
acetophenone	9.9[37]	−1.474 V[37,39]	−1.655 eV	−0.782 eV
anthraquinone	5.3[37]	−0.45 V[40]	−2.407 eV	−1.402 eV

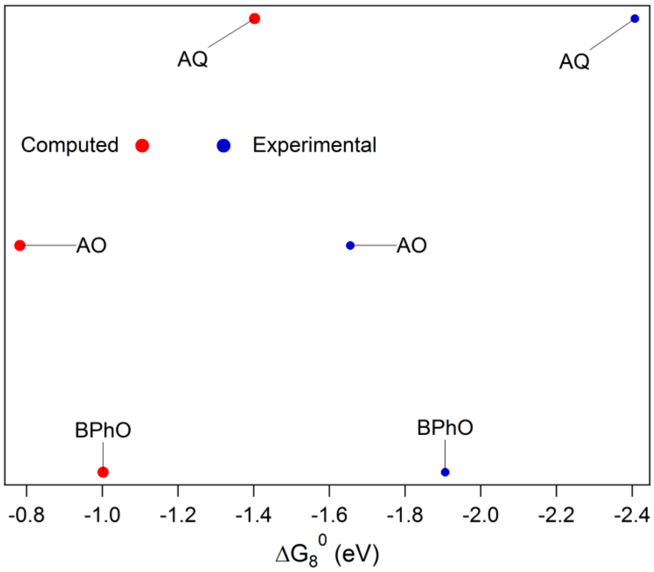

Figure S16.2 A plot of the calculated and experimental standard free energy changes of Reaction 8 in water for anthraquinone (AQ), acetophenone (AO), and benzophenone (BPhO).

Electron Transfer Reaction. We also separated the electron transfer reaction (Reaction 4b) into two half-reactions:

$$M^{\bullet-}_{(liq)} \rightarrow M_{(liq)} + e^-_{(gas)} \quad (5)$$

$$e^-_{(gas)} + RH^+_{2\,(liq)} \rightarrow H^\bullet_{(gas)} + RH_{(liq)} \quad \text{(S16.4)}$$

The ΔG^0 of the electron transfer reaction is the sum of the ΔG^0 of reactions 5 and S16.4; the calculation results are in Table 16.4. Again, the ΔG_5^0 is estimated based on the reduction potentials give in Table 3. The ΔG^0 of reaction S16.4 was computed by MP2/6-31G(d) with the geometry optimized by B3LYP/6-31G(d) in the PCM solvation model for THF and corrections for the BSSE. The ΔG^0 of reaction S16.4 are −1.674 and −2.970 eV for the solvated proton stabilized by one and two THF molecules, respectively. The calculation results are given in Table S15.4. In THF, a possible structure of the solvated proton is that the proton solvated by two THF, $H^+(THF)_2$. Based on the calculation results for $H^+(THF)_2$, the electron transfer reaction (Reaction 4b) may be endoergic. This result implies that annihilation of anions in THF is possibly due to the proton transfer reaction (Reaction 4a).

Table S16.4 The computed standard free energy change (ΔG^0) from MP2/6-31G(d)//B3LYP/6-31G(d)/PCM based on the reduction potential for the electron transfer reaction (Reaction 4b) if the proton solvated by one or two THF molecules.

Name	1 THF	2 THF
	ΔG^0 (eV)	ΔG^0 (eV)
F_1	−0.898	0.398
F_2	−0.543	0.753
F_3	−0.367	0.929
F_4	−0.325	0.971
dibenzofuran	−0.774	0.522
fluoranthene	−0.050	1.246
phenanthrene	−0.740	0.556
1-methylpyrene	−0.350	0.946
biphenyl	−0.870	0.426
p-terphenyl	−0.640	0.656
terthiophene	−0.385	0.911
fluorobenzene	−1.477	−0.181
o-terphenyl	−0.820	0.476
4-cyano-4’-n-pentyl-p-terphenyl	−0.108	1.188
p-dinitrobenzene	1.085	2.381
benzophenone	−0.196	1.100
anthraquinone	0.924	2.220
tetrachloro-*p*-benzoquinone	1.870	3.166
acetophenone	−0.230	1.066
2,3-dichloro-5,6-dicyano-*p*-benzoquinone	2.348	3.644
4-nitro-*p*-terphenyl	0.590	1.886
2,3-dicynao-*p*-benzoquinone	2.123	3.419
tetracynaoethene	1.910	3.206

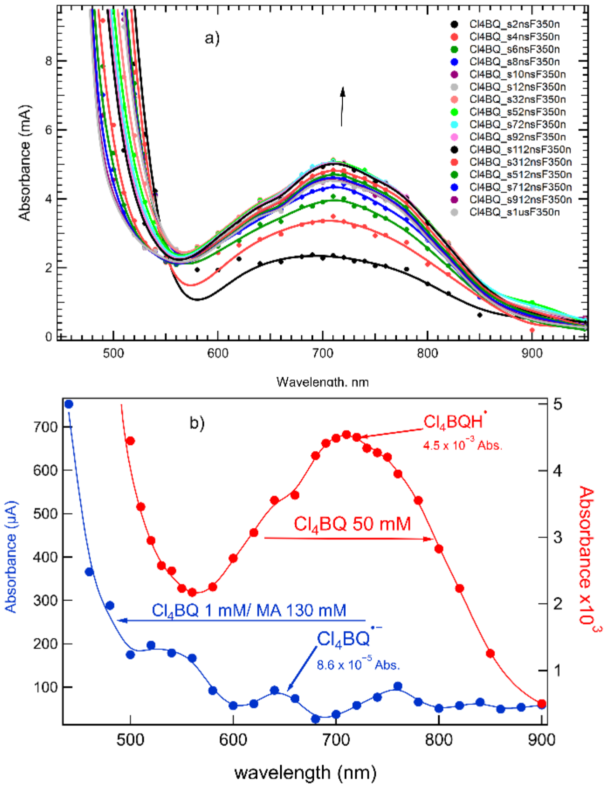

Figure S17 Absorption spectra from the pulse radiolysis of a) 50 mM tetrachloro-*p*-benzoquinone (Cl_4BQ). The absorbance of the $Cl_4BQH^{\cdot}$ radical grows in as Cl_4BQ anions (peaking about 420 nm) decay. This peak can not be observed at the high concentration of Cl_4BQ. b) (●) 1 mM Cl_4BQ +130 mM maleic anhydride (MA) and (●) 50 mM Cl_4BQ in THF, both at 1.8 μs after the electron pulse. The concentration of Cl_4BQ anions should be almost identical in the two spectra, but in 50 mM Cl_4BQ geminate electrons captured by Cl_4BQ recombine with solvated protons to create $Cl_4BQH^{\bullet}$ radicals yielding the broad, weak absorption band peaking ~720 nm that grows in with a time constant of ~10 ns. The presence of a low energy transition is predicted by DFT (see below). The large, 130 mM, concentration of MA captures most electrons from pulse radiolysis in <<1 ns and then the electrons transfer to Cl_4BQ. Most geminate recombination occurs between $MA^{\bullet-}$ and solvated protons. The longer-lived free $MA^{\bullet-}$ transfer their electrons to Cl_4BQ. Therefore the blue spectrum in (●) shows only $Cl_4BQ^{\bullet-}$ absorption with almost no absorption band at 700 nm.

TD-DFT($Cl_4BQH^{\bullet}$) results in THF using `B3LYP/6-31g(d)`:

Excited State 1: 2.065-A 1.7117 eV 724.34 nm f=0.0000 <S**2>=0.816

Excited State 2: 2.032-A 2.0289 eV 611.09 nm f=0.0049 <S**2>=0.782

Excited State 3: 2.078-A 3.0133 eV 411.45 nm f=0.0579 <S**2>=0.829

Excited State 4: 2.035-A 3.7141 eV 333.82 nm f=0.1263 <S**2>=0.786

Energies of transitions in this calculation may have limited accuracy due to spin contamination.

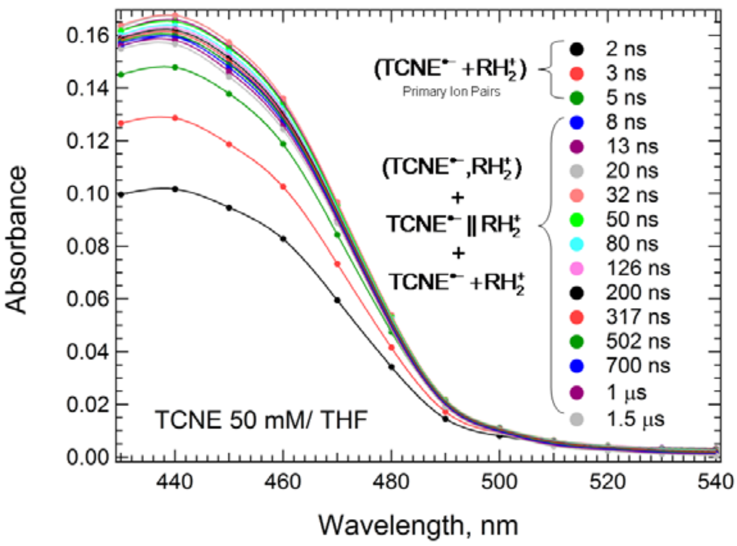

Figure S18 Transient spectra of tetracyanoethylene radical anion ($TCNE^{\bullet-}$) in THF, where the primary ion pairs ($TCNE^{\bullet-}+RH_2^+$) at varied distances are expected to recombine to form ($TCNE^{\bullet-},RH_2^+$) contact ion pairs (CIP), $TCNE^{\bullet-}||RH_2^+$ solvent separated ion pairs (SSIP) and separate $TCNE^{\bullet-}+RH_2^+$ (free ions). $TCNE^{\bullet-}$ was produced by the pulse radiolysis in THF with 50 mM of TCNE. No decay of $TCNE^{\bullet-}$ is observed only growth ($k_1=3.87\text{x}10^8$ s^{-1}; $k_{Bi}=7.7\text{x}10^9$ $M^{-1}s^{-1}$) as TCNE captures solvated electrons. There is no detectable difference of the spectra with time, indicating that the absorption spectra primary ion pairs, CIP, SSIP and free ions may be identical. According to kinetic traces of $BPhO^{\bullet-}$, most primary ion pairs become CIP, SSIP and free ions in THF after ~8 ns

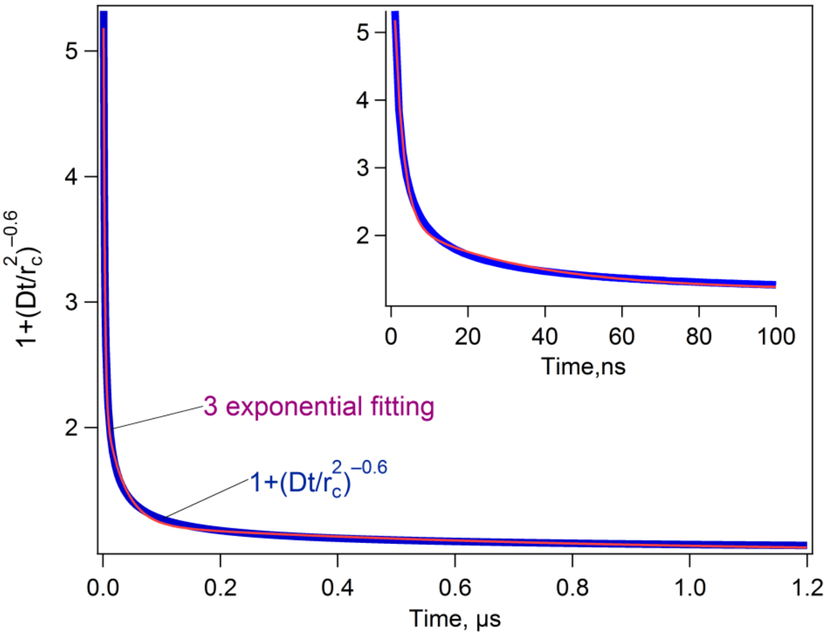

Figure S19. Plots of $1+(Dt/r_c^2)^{-0.6}$ (blue) for $Dt/r_c^2 < 32$ compared to a three-exponential function (red), $1+4.70\ \exp(-4.56\times10^8 t)+1.01\ \exp(-3.16\times10^7 t)+0.23\ \exp(-1.35\times10^6 t)$ in THF show a good agreement. The $1+(Dt/r_c^2)^{-0.6}$ is an empirical function reported by Van de Ende,[1] which can well describe the geminate ion recombination in CCl_4. Here D is the mutual diffusion coefficient between the anion and cation, r_c=7.3 nm is the Onsager radius. We estimate the mutual diffusion coefficient with the self-diffusion coefficient of THF (3.0×10^{-5} cm^2/s)[2] and diffusion coefficient of benzophenone (1.65×10^{-5} cm^2/s).[3]

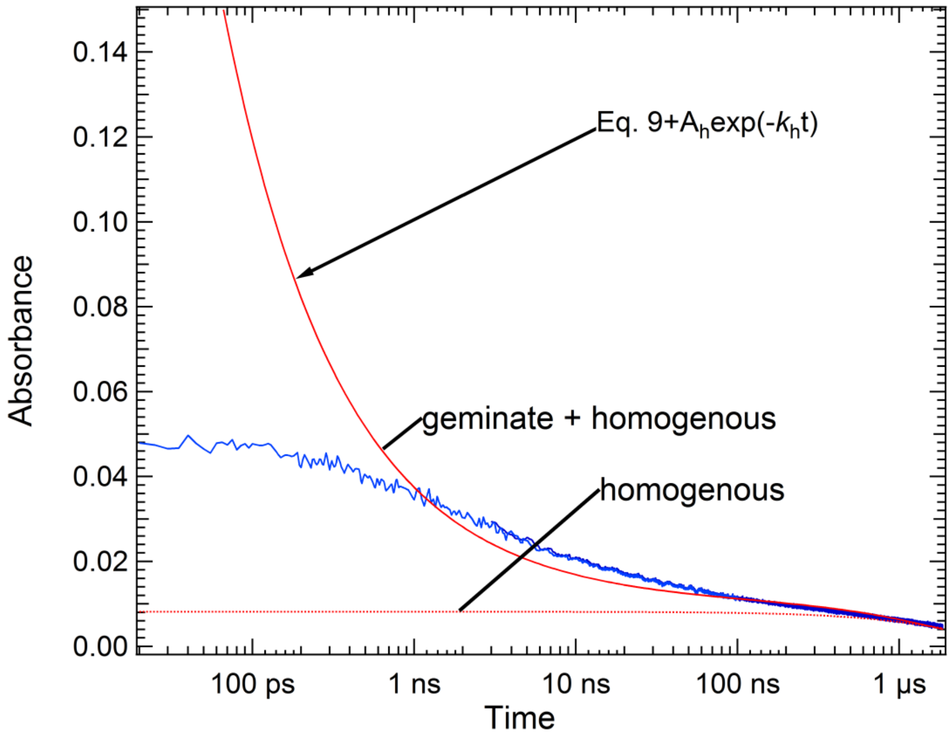

Figure S20. Decay of transient absorption from 200 mM of benzophenone in THF compared with the function of Van den Ende and coworkers[1] (eq. 9), $W(\tau)=(1+0.6\ \tau^{-0.6})$ and $\tau=Dt/r_c^2$. The solid red line is geminate decay according to eq. 9 plus a homogeneously decaying fraction described by a single exponential, $A_h\ \exp(-k_h t)$ fit to the data; $D=4.6\times10^{-5}$ cm^2/s, $r_c=7.6$ nm, $k_h=5.31\times10^5$ s^{-1}, and $A_h=0.01$. The dashed red line is the homogeneous fraction only. The arrow at t=600 ps is the time after which eq 9 was found to be applicable in CCl_4. The data at earlier times depart substantially, but substantial differences remain also a longer times.

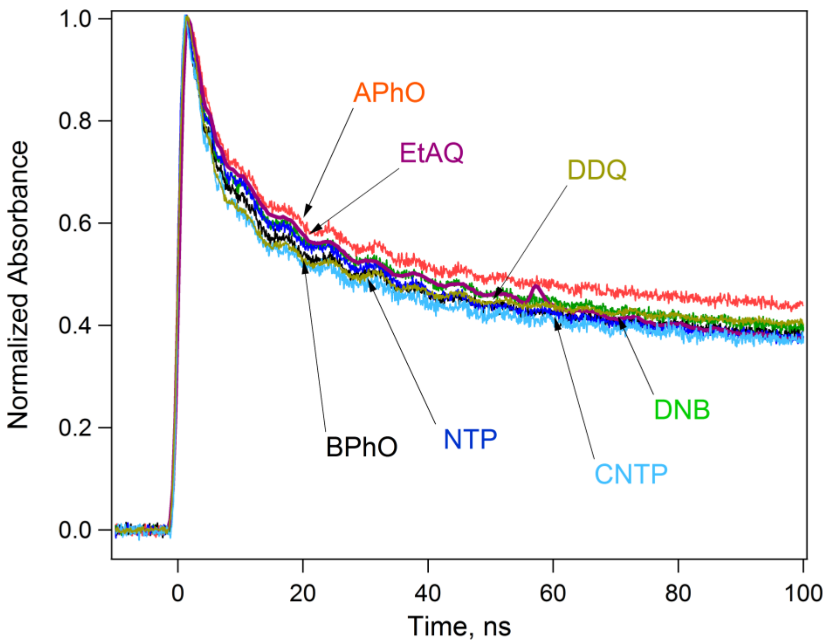

Figure S21. Kinetic traces of benzopheone (BPhO), *p*-dinitrobenzene (DNB), 2-ethyl-9,10-anthraquinone (EtAQ), 4-nitro-*p*-terphenyl (NTP), 2,3-dichloro-5,6-dicyano-*p*-benzoquinone, (DDQ), 4-cyano-4'-*n*-pentyl-*p*-terphenyl (CNTP), and acetophenone (APhO) show nearly identical geminate decay.

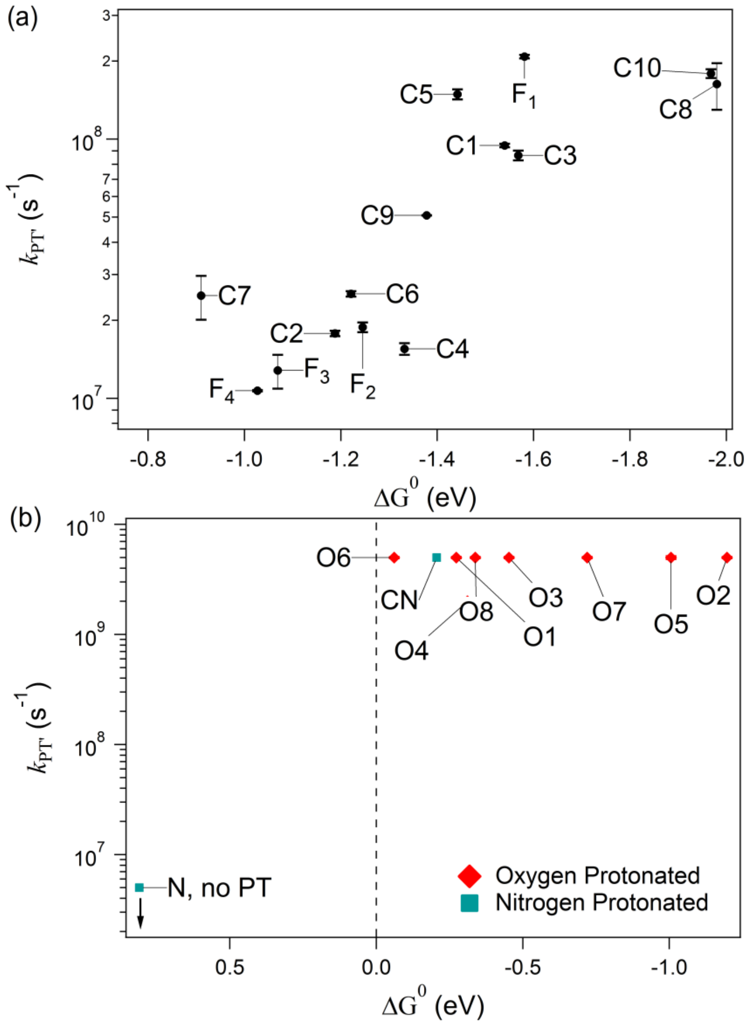

Figure S22 Plots of the measured proton transfer rate ($k_{PT'}$) vs. the estimated standard free energy change (ΔG^0) for the proton transfer reaction for (a) C protonated, and (b) N and O protonated molecules. k_{MPT} for the N and O protonated molecules are all lower limits, except for TCNE, which is an upper limit. The lower arror means that no occurrence of the proton transfer.

References

1. van den Ende, C. A. M.; Luthjens, L. H.; Warman, J. M.; Hummel, A., Geminate Ion Recombination in Irradiated Liquid Ccl4: As Observed by Means of Microwave and Optical Absorption Pulse Radiolysis and Compared with Calculations Based on a Single Ion Pair Model. *Radiation Physics and Chemistry* **1982**, *19*, 455-466.
2. Hayamizu, K.; Aihara, Y.; Arai, S.; Garcia, Pulse-Gradient Spin-Echo 1h, 7li, and 19f Nmr Diffusion and Ionic Conductivity Measurements of 14 Organic Electrolytes Containing Lin(So2cf3)2. *Journal of Physical Chemistry B* **1999**, *103*, 519-524.
3. Tsierkezos, N., Investigation of the Electrochemical Reduction of Benzophenone in Aprotic Solvents Using the Method of Cyclic Voltammetry. *Journal of Solution Chemistry* **2007**, *36*, 1301-1310.

4. Bockrath, B.; Dorfman, L. M., Pulse Radiolysis Studies. Xxii. Spectrum and Kinetics of the Sodium Cation-Electron Pair in Tetrahydrofuran Solutions. *Journal of Physical Chemistry* **1973**, *77*, 1002-1006.
5. Bhattacharyya, D. N.; Lee, C. L.; Smid, J.; Szwarc, M., Studies of Ions and Ion Pairs in Tetrahydrofuran Solution. Alkali Metal Salts of Tetraphenylboride. *Journal of Physical Chemistry* **1965**, *69*, 608-611.
6. Saeki, A.; Kozawa, T.; Ohnishi, Y.; Tagawa, S., Reactivity between Biphenyl and Precursor of Solvated Electrons in Tetrahydrofuran Measured by Picosecond Pulse Radiolysis in near-Ultraviolet, Visible, and Infrared. *Journal of Physical Chemistry A* **2007**, *111*, 1229-1235.
7. Monchick, L.; Magee, J. L.; Samuel, A. H., Theory of Radiation Chemistry. Iv. Chemical Reactions in the General Track Composed of N Particles. *J. Chem. Phys.* **1957**, *26*, 935-941.
8. Bartels, D. M.; Cook, A. R.; Mudaliar, M.; Jonah, C. D., Spur Decay of the Solvated Electron in Picosecond Radiolysis Measured with Time-Correlated Absorption Spectroscopy. *J. Phys. Chem. A* **2000**, *104*, 1686-1691.
9. Cook, A. R., Personal Communication. 2013.
10. Cook, A. R.; Shen, Y., Optical Fiber-Based Single-Shot Picosecond Transient Absorption Spectroscopy. *Review of Scientific Instruments* **2009**, *80*, 073106.
11. Lam, K. Y.; Hunt, J. W., Picosecond Pulse Radiolysis—Vi. Fast Electron Reactions in Concentrated Solutions of Scavengers in Water and Alcohols. *International Journal for Radiation Physics and Chemistry* **1975**, *7*, 317-338.
12. Wolff, R. K.; Aldrich, J. E.; Penner, T. L.; Hunt, J. W., Picosecond Pulse Radiolysis. V. Yield of Electrons in Irradiated Aqueous Solution with High Concentrations of Scavenger. *Journal of Physical Chemistry* **1975**, *79*, 210-219.
13. Sreearunothai, P.; Asaoka, S.; Cook, A. R.; Miller, J. R., Length and Time-Dependent Rates in Diffusion-Controlled Reactions with Conjugated Polymers. *Journal of Physical Chemistry A* **2009**, *113*, 2786-2795.
14. Cook, A. R.; Sreearunothai, P.; Asaoka, S.; Miller, J. R., Sudden, "Step" Electron Capture by Conjugated Polymers. *Journal of Physical Chemistry A* **2011**, *115*, 11615-11623.
15. Jones, G.; Griffin, S. F.; Choi, C. Y.; Bergmark, W. R., Electron Donor-Acceptor Quenching and Photoinduced Electron Transfer for Coumarin Dyes. *Journal of Organic Chemistry* **1984**, *49*, 2705-2708.
16. Furuuchi, H.; Arai, T.; Kuriyama, Y.; Sakuragi, H.; Tokumaru, K., Factors Distinguishing One-Way and Two-Way Photoisomerization of Aromatic Olefins. Effects of Substituents on Triplet Energy Surfaces of 8-Fluoranthenylethylenes. *Chem. Phys. Lett.* **1989**, *162*, 211-216.
17. Zaikowski, L., et al., Polarons, Bipolarons, and Side-by-Side Polarons in Reduction of Oligofluorenes. *J. Am. Chem. Soc.* **2012**, *134*, 10852-10863.
18. Legros, B.; Vandereecken, P.; Soumillion, J. P., Electron Transfer Photoinduced from Naphtholate Anions: Anion Oxidation Potentials and Use of Marcus Free Energy Relationships. *Journal of Physical Chemistry* **1991**, *95*, 4752-4761.
19. Ruoff, R. S.; Kadish, K. M.; Boulas, P.; Chen, E. C. M., Relationship between the Electron Affinities and Half-Wave Reduction Potentials of Fullerenes, Aromatic Hydrocarbons, and Metal Complexes. *Journal of Physical Chemistry* **1995**, *99*, 8843-8850.
20. Wagman, D. D.; Evans, W. H.; Parker, V. B.; Schumm, R. H.; Halow, I.; Bailey, S. M.; Churney, K. L.; Nuttall, R. L., The Nbs Tables of Chemical Thermodynamic Properties *Journal of Physical and Chemical Reference Data, Supplment 1* **1982**, *11*.

21. Gerdil, R.; Lucken, E. A. C., A Polarographic and Spectroscopic Study of Dibenzothiophene and Some of Its Isologs. *Journal of the American Chemical Society* **1966**, *88*, 733-737.
22. Streitwieser, A.; Schwager, I., A Molecular Orbital Study of the Polargraphic Reduction in Dimethylformamide of Unsubstituted and Methyl-Substituted Aromatic Hydricarbonds. *J. Phys. Chem.* **1962**, *66*, 2316-2320.
23. Shriver, D. F.; Smith, D. E.; Smith, P., Reduction Potentials and Electronic Structures of Phenyl-Substituted Borazines. *Journal of the American Chemical Society* **1964**, *86*, 5153-5160.
24. Meerholz, K.; Heinze, J., Electrochemical Solution and Solid-State Investigations on Conjugated Oligomers and Polymers of the α-Thiophene and the *P*-Phenylene Series. *Electrochim. Acta* **1996**, *41*, 1839-1854.
25. Marasas, R. A.; Iyoda, T.; Miller, J. R., Benzene Radical Ion in Equilibrium with Solvated Electrons. *The Journal of Physical Chemistry A* **2003**, *107*, 2033-2038.
26. Shalev, H.; Evans, D. H., Solvation of Anion Radicals: Gas-Phase Versus Solution. *Journal of the American Chemical Society* **1989**, *111*, 2667-2674.
27. Prince, R. C.; Gunner, M. R.; Dutton, P. L., *In Function of Quinones in Energy Conserving Systems*; Academic Press: New York, 1982.
28. Connors, T. F.; Rusling, J. F.; Owlia, A., Determination of Standard Potentials and Electron-Transfer Rates for Halobiphenyls from Electrocatalytic Data. *Analytical Chemistry* **1985**, *57*, 170-174.
29. Hansen, R. L.; Toren, P. E.; Young, R. H., Nitro-P-Terphenyls. Ii. The Relation between Charge-Transfer Properties and Polarographic Oxidation and Reduction Potentials. *Journal of Physical Chemistry* **1966**, *70*, 1653-1657.
30. Gross-Lannert, R.; Kaim, W.; Olbrich-Deussner, B., Electron Delocalization in Molecule-Bridged Polymetallic Systems. Unique Neutral Complexes of Tcne or Tcnq and up to Four Organometallic Fragments (C5r5)(Co)2mn. *Inorganic Chemistry* **1990**, *29*, 5046-5053.
31. Bard, A. J.; Faulkner, L. R., Electrochemical Methods: Fundamentals and Applications. Wiely: 2001; p Cover.
32. Kukharenko, S. V.; Strelets, V. V., One-Electron Cryoelectrochemical Reduction of Benzene. *Soviet Electrochemistry* **1988**, *24*, 1271-1272.
33. Connelly, N. G.; Geiger, W. E., Chemical Redox Agents for Organometallic Chemistry. *Chemical Reviews* **1996**, *96*, 877-910.
34. Berho, F.; Rayez, M.-T.; Lesclaux, R., Uv Absorption Spectrum and Self-Reaction Kinetics of the Cyclohexadienyl Radical, and Stability of a Series of Cyclohexadienyl-Type Radicals. *Journal of Physical Chemistry A* **1999**, *103*, 5501-5509.
35. Collyer, S. M.; McMahon, T. B., Proton Affinity of Water. A Scale of Gas-Phase Basicities Including Ethylene and Water from Ion Cyclotron Resonance Proton Transfer Equilibrium Measurements. *J. Phys. Chem.* **1983**, *87*, 909-911.
36. Palascak, M. W.; Shields, G. C., Accurate Experimental Values for the Free Energies of Hydration of H+, Oh-, and H3o+. *J. Phys. Chem. A* **2004**, *108*, 3692-3694.
37. Rao, P. S.; Hayon, E. Redox Potentials of Free Radicals. I. Simple Organic Radicals. 0002-7863, 1974.
38. Reduction potentials in Ref 31 doesn't give reference electrode so reduction potential of BPhO is based on the reduction potential difference between AQ and BPhO from Ref 31 and reduction potential (vs. SCE) of AQ reported in Ref 34 in water.
39. Reduction potentials in Ref 31 are not giving reference electrode so reduction potential of acetophenone is based on difference of reduction potentials between acetophenone and anthraquinone (AQ) from Ref 31 and reduction potential (vs. SCE) of AQ reported in Ref 34 in water.

40. Hayano, S.; Fujihira, M., The Effect of Water on the Reduction Potentials of Some Aromatic Compounds in the Dmf-Water System. *Bulletin of the Chemical Society of Japan* **1971**, *44*, 2051-2055.